International Journal of GEOMATE, May, 2025 Vol.28, Issue 129, pp.84-96
ISSN: 2186-2982 (P), 2186-2990 (O), Japan, DOI: https://doi.org/10.21660/2025.129.4949
Geotechnique, Construction Materials and Environment

THE IMPORTANCE OF HOOPS AS SHEAR AND CONFINEMENT REINFORCEMENT IN EXTERIOR BEAM–COLUMN JOINTS

*Altho Sagara[1], Iswandi Imran[1], Erwin Lim[1], Patria Kusumaningrum[1]

[1]Civil Engineering Department, Institut Teknologi Bandung, Indonesia

*Corresponding Author, Received: 17 March 2025, Revised: 20 April 2025, Accepted: 28 April 2025

ABSTRACT: This study examines 59 exterior beam–column joint (BCJ) specimens from previous research to evaluate the influence of joint hoops on seismic performance. The analysis indicates that joint hoops become increasingly important as the drift ratio increases. To further validate this outcome, experimental tests are conducted on two specimens, namely A-1-100 (with hoops) and A-1-0 (without hoops). The results show that joint hoops have little influence on joint resistance at lower drift ratios. However, as drift ratio increases, side hoops contribute to shear resistance by controlling crack propagation along a joint's sides. The influence of the side hoops becomes more noticeable but gradually diminishes due to bond degradation. On the other hand, back hoops primarily provide confinement by restricting joint dilation, particularly at higher drift ratios. As damage accumulates, back hoops play a crucial role in maintaining joint integrity and delaying excessive deformation. The findings indicate that joint hoop detailing in exterior BCJs may be optimized without significantly compromising seismic performance, thus offering potential improvements for both new construction and retrofit design. It also contributes to a deeper understanding of the transition from truss to strut mechanisms as drift ratio increases, providing valuable insights for refining analytical models and supporting performance-based design approaches.

Keywords: Exterior beam–column joint, Experimental testing, Shear resistance, Confinement

1. INTRODUCTION

The role of an exterior beam–column joint (BCJ) is crucial to the overall seismic performance of reinforced-concrete (RC) structures, as the joint experiences complex stress conditions under lateral loads. Therefore, ensuring proper reinforcement and confinement in this joint is essential for maintaining adequate strength, ductility, and energy-dissipation capacity. A key reinforcement element in a BCJ is the joint hoops, which help improve shear strength, provide confinement, and enhance overall seismic behavior. Despite their importance, closely spaced reinforcement in joint regions often leads to steel congestion, making construction more challenging. This issue has prompted researchers to reassess the role of joint hoops and explore ways to optimize reinforcement detailing.

ACI 318-25 [1] adopts joint shear strength provisions from ACI 352R-02 [2] for joints subjected to inelastic deformation due to seismic loading. However, the code does not explicitly account for joint hoops in shear strength calculations. This approach is based on studies by Meinheit and Jirsa [3], as well as Hirosawa [4], which suggest that, once the minimum required reinforcement for confinement is provided, additional transverse reinforcement does not significantly affect joint shear strength. These findings indicate that shear strength is primarily influenced by joint strength and geometry rather than the number of hoops.

The role of joint hoops in exterior BCJs remains a subject of ongoing discussion. Some studies suggest that joints can achieve satisfactory seismic performance even with reduced confinement reinforcement, provided key design aspects—such as adequate anchorage and sufficient shear strength—are met. Hwang et al., Al Osta et al., Castro and Imai, Alaee and Li, Hwang and Park, Huang et al., Hakuto et al., and Kuang and Wong [5–12] found that exterior BCJs containing fewer joint hoops than those specified by ACI 318-25 [1] can still perform effectively under seismic loading. Meanwhile, other studies emphasize the crucial role of joint hoops in line with ACI 318-25 [1] provisions. For example, Lee and Chang, Ehsani and Wight, Canbolat and Wight, and Lee and Yu [13–16] reported that joint hoops enhance ductility, shear strength, and energy dissipation capacity, particularly under high drift ratio demands. These contrasting results highlight the need for a more in-depth investigation to determine the specific conditions under which joint hoops actively contribute to shear resistance and confinement in exterior BCJs. Accordingly, a comprehensive analysis of existing databases and experimental studies is essential to better understand when and how joint hoops influence seismic performance. By examining the progression of shear resistance and confinement effects, a clearer understanding of the contribution of joint hoops can be developed to improve seismic performance.

Park and Paulay [17] identified two shear

resistance mechanisms in BCJs: the diagonal concrete strut and the truss mechanism. The diagonal concrete strut transfers the shear through compression between the joint's compressed corners, while the truss mechanism relies on stirrup ties and longitudinal reinforcement to resist shear forces. These mechanisms behave differently under cyclic loading, thereby influencing joint performance in both the elastic and inelastic stages.

The following sections present the significance of this research, a review of an experimental database on previous research, and the experimental program, followed by the analysis and discussion of key findings, including the contribution of truss and strut mechanisms in joint behavior. The paper concludes with practical implications and suggestions for future research.

2. RESEARCH SIGNIFICANCE

This study aims to provide a clearer understanding of the role of joint hoops in BCJs through an in-depth analysis of existing experimental data and additional testing. The findings will clarify whether joint hoops primarily function as confinement reinforcement or contribute to shear resistance under different loading conditions, while also providing practical guidance for optimizing reinforcement detailing in seismic design. By addressing the balance between structural performance and construction challenges due to reinforcement congestion, the study enhances BCJ design efficiency. It also clarifies ACI 318 provisions, helping engineers make informed decisions to improve seismic detailing and structural resilience.

3. EXPERIMENTAL DATABASE OF PREVIOUS STUDIES

This study used an experimental database consisting of 59 previously tested exterior BCJ specimens [5–21] to conduct an exploratory investigation. The database covers a range of concrete strengths (f_c') from 21 to 90 MPa, yield strengths of reinforcement (f_y) from 326 to 843 MPa, longitudinal reinforcement ratios in the beam between 1% and 4%, and in the column between 1% and 3%. The specimens include both cases with and without joint hoops. The analysis focused on assessing the installed joint hoops relative to the minimum requirements specified in ACI 318-25 [1]. To determine whether the provided confinement reinforcement met the standard, the total required area of confining reinforcement (A_{sh}) was calculated using the following equation:

$$A_{sh-ACI} = \max\ [\,0.3\ \frac{f_c'}{f_{yh}}\left(\frac{A_g}{A_{ch}}-1\right) s\ b_c;\ 0.09\ \frac{f_c'}{f_{yh}}\ s\ b_c;\ 0.2\ k_f k_n \frac{P_u}{f_{yt}A_{ch}}\,] \quad (1)$$

where f_{yh} is the yield strength of joint hoops, A_g represents the gross column section area, and A_{ch} denotes the section area of the column core. The variable s is the vertical spacing of joint hoops, while b_c is the column width in the perpendicular direction. Additionally, k_f and k_n represent the concrete strength factor and confinement effectiveness factor, respectively, which must be calculated for columns subjected to high axial loads.

To evaluate the influence of joint hoops on the deformability of BCJs, this study examined how variations in hoop quantity relate to lateral drift capacity and, more critically, to the overall ductility of the specimens. The maximum drift ratio was calculated as the ratio of the maximum lateral displacement observed during testing to the effective height of the specimen, which could correspond to either the column height or beam length, depending on the specific test setup adopted in each experimental program. On the other hand, ductility, denoted by the symbol μ, was defined as the ratio between the drift ratio at maximum strength (D_{max}) and the drift ratio at first yielding (D_y). Here, D_y represents the drift ratio at which the specimen initially exhibited yielding behavior, typically associated with the onset of inelastic deformation, while D_{max} corresponds to the drift ratio at which the peak lateral load was attained before strength degradation occurs. These two deformation-based parameters were crucial for providing a comprehensive understanding of the specimens' deformability. They played a key role in assessing the joints' ability to withstand large deformations without significant strength loss, as well as in evaluating their energy dissipation capacity under seismic loading.

The findings presented in Figure 1(a) indicate that specimens with fewer joint hoops than the required amount were still able to accommodate significant deformation, particularly in the studies by Hwang *et al*., Castro and Imai, and Bindhu and Sukumar [5,7,20]. This outcome is primarily attributed to the satisfactory performance of the strong-column–weak-beam (SCWB) mechanism and adequate joint strength, which allowed the specimens to exceed expectations despite the insufficient number of joint hoops. Similarly, Wibowo and Cahyani [22] emphasized the critical role of joint hoops in providing confinement, particularly at large drift ratios. This was further demonstrated in the specimens examined in this study, where the presence of joint hoops effectively contributed to maintaining structural integrity under extreme loading conditions. The numerical data supporting these observations are presented in Table

1.

Although studies [5,7,20] showed that fewer joint hoops could still accommodate deformation, others [13–15] reported brittle failures due to inadequate anchorage and torsional effects, even with more hoops. Canbolat and Wight [15] emphasized that joint hoops alone could not prevent failure when other critical factors are insufficient. As illustrated in Figure 1(b), joint hoops are not a substitute for proper anchorage, sufficient joint strength, and an adequate moment ratio, all of which must be fulfilled together to ensure reliable confinement and maintain structural integrity.

Despite these findings from the existing database, most specimens demonstrated that achieving a fully compliant number of joint hoops was not always essential for realizing a ductile failure pattern. This was particularly evident when evaluated based on ASCE 7-16 criteria (drift ratio > 2% for strength under a design-basis earthquake (DBE) and drift ratio > 3% for deformability under a Risk-Targeted Maximum Considered Earthquake (MCE_R), as prescribed by ACI 318-25 [1]. Based on these observations, the results indicated the potential for optimizing joint hoop detailing in exterior BCJs while maintaining seismic performance.

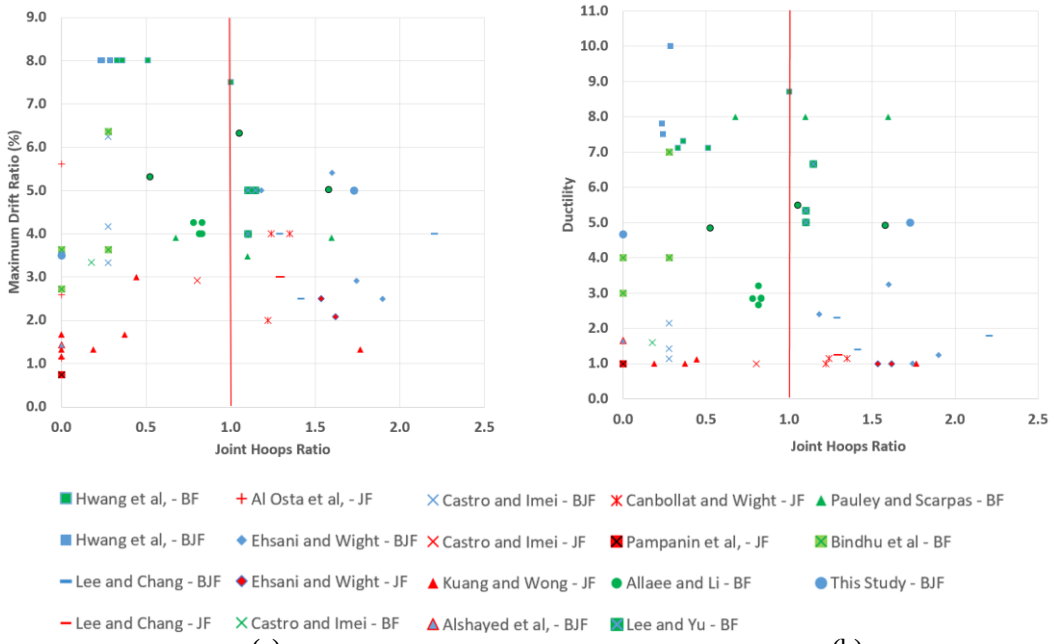

(a) (b)

Fig.1 Relationship between joint hoops ratio and (a) maximum drift ratio, and (b) ductility, based on experimental database.

Table 1. Database of joint hoops ratio, drift ratio values, and failure modes.

Author	Specimen	Joint Hoops Ratio ($A_{sh\text{-}exp}/A_{sh\text{-}ACI}$)	D_y (%)	D_{max} (%)	μ (D_{max}/D_y)	Failure Mode
Hwang *et al.*, 2005 [5]	3T3	0.29	0.80	8.00	10.00	BJF
	2T4	0.24	1.07	8.00	7.50	BJF
	1T44	0.23	1.03	8.00	7.80	BJF
	3T44	1.00	0.86	7.50	8.70	BF
	3T4	0.51	1.13	8.00	7.10	BF
	2T5	0.33	1.13	8.00	7.10	BF
	1T55	0.36	1.10	8.00	7.30	BF
Lee and Chang, 2017 [13]	A5	1.29	1.74	4.00	2.30	BJF
	B5	1.42	1.79	2.50	1.40	BJF
	B3	2.21	2.22	4.00	1.80	BJF

Table 1. (continued)

Author	Specimen	Joint Hoops Ratio ($A_{sh\text{-}exp}/A_{sh\text{-}ACI}$)	D_y (%)	D_{max} (%)	μ (D_{max}/D_y)	Failure Mode
Lee and Chang, 2017 [13]	C5	1.29	2.40	3.00	1.25	JF
	C3	2.14	2.40	3.00	1.25	BJF
Al Osta *et al.*, 2018 [6]	SP4	0.00	2.58	2.58	1.00	JF
	SP5	0.00	5.62	5.62	1.00	JF
	SP7	0.00	1.12	1.12	1.00	JF
Ehsani and Wight, 1985 [14]	1B	1.62	2.08	2.08	1.00	JF
	2B	1.53	2.50	2.50	1.00	JF
	3B	1.74	2.92	2.92	1.00	BJF
	4B	1.60	1.67	5.42	3.25	BJF
	5B	1.90	2.00	2.50	1.25	BJF
	6B	1.18	2.08	5.00	2.40	BJF
Castro and Imei, 2004 [7]	No. 1	0.28	2.92	6.25	2.14	BJF
	No. 5	0.80	2.92	2.92	1.00	JF
	No. 7	0.28	2.92	4.17	1.43	BJF
	No. 10	0.28	2.92	3.33	1.14	BJF
	No. 11	0.18	2.08	3.33	1.60	BF
Kuang and Wong, 2011 [12]	BS-450	0.00	1.17	1.17	1.00	JF
	BS-450-H1T10	0.37	1.67	1.67	1.00	JF
	BS-450-H2T10	0.44	2.67	3.00	1.13	JF
	BS-600	0.00	1.33	1.33	1.00	JF
	BS-600-H2T8	0.19	1.33	1.33	1.00	JF
	BS-600-H4T8	1.77	1.33	1.33	1.00	JF
	BS-L	0.00	1.67	1.67	1.00	JF
	BS-LL	0.00	1.67	1.67	1.00	JF
Alshayed *et al.*, 2010 [18]	EC 1	0.00	0.86	1.43	1.67	BJF
Canbollat and Wight, 2008 [15]	Specimen 1	1.35	3.50	4.00	1.14	JF
	Specimen 2	1.24	3.50	4.00	1.14	JF
	Specimen 3	1.22	2.00	2.00	1.00	JF
Pampanin *et al.*, 2002 [19]	T1	0.00	0.75	0.75	1.00	JF
Alaee and Li, 2017 [8]	EN80	0.82	1.50	4.00	2.67	BF
	EH80	0.82	1.25	4.00	3.20	BF
	EH80A	0.78	1.50	4.25	2.83	BF
	EH60	0.83	1.40	4.00	2.86	BF
	EH60A	0.83	1.50	4.25	2.83	BF
Lee and Yu, 2009 [16]	W0	1.15	0.75	5.00	6.67	BF
	W0-M1	1.10	0.75	4.00	5.33	BF
	W0-M2	1.10	1.00	5.00	5.00	BF
Paulay and Scarpas, 1981 [21]	UNIT 1	1.10	2.30	3.48	8.00	BF
	UNIT 2	1.60	2.04	3.91	8.00	BF
	UNIT 3	0.68	2.04	3.91	8.00	BF
Bindhu *et al.*, 2009 [20]	A1-456	0.00	0.91	3.64	4.00	BF
	A2-456	0.00	0.91	2.73	3.00	BF
	A1-13920	0.28	0.91	6.36	7.00	BF
	A2-13920	0.28	0.91	3.64	4.00	BF

Table 1. (continued)

Author	Specimen	Joint Hoops Ratio ($A_{sh\text{-}exp}/A_{sh\text{-}ACI}$)	D_y (%)	D_{max} (%)	μ (D_{max}/D_y)	Failure Mode
This Study	A-1-100	1.73	1.00	5.00	5.00	BJF
	A-1-0	0	0.75	3.50	4.67	BJF

4. EXPERIMENTAL PROGRAM

A clearer understanding of the role of joint hoops is essential for determining how and when they contribute to shear resistance and confinement. To achieve this, an experimental study was conducted on two half-scale exterior BCJ specimens to evaluate their structural response under cyclic lateral loading. The adopted scale and testing approach comply with the similitude requirements and recommendations in ACI 374.1-05 [23].

This investigation aimed to provide deeper insights into the influence of joint hoops on shear strength, confinement effectiveness, and seismic performance. The study focused on two specimens: A-1-100 (with hoops) and A-1-0 (without hoops). Both specimens had identical dimensions and reinforcement details, as shown in Figure 2. The column had a cross-section of 330 × 330 mm, while the beam measured 400 mm in depth and 330 mm in width. Additionally, the lengths of the column and beam were 1,610 mm and 2,250 mm, respectively, corresponding to the inflection points of structural members in a typical multi-story building. These dimensions were adjusted to accommodate the measurements of the testing machine.

The transverse beam was also constructed with the same dimensions as the main beam and a length of 330 mm, as required by ACI 318-25 [1], to provide an outer confinement effect, ensuring a realistic representation of BCJs commonly found in practice. To assess the behavior of non-seismic BCJs, all specimens were intentionally designed with inadequate joint shear strength, as defined by the Building Code Requirements for Structural Concrete and Commentary (ACI 318-25) [1]. This approach aimed to highlight the performance deficiencies and failure mechanisms that may arise in joints lacking adequate seismic reinforcement, particularly under lateral cyclic loading conditions.

The average compressive strengths of concrete (f_c') measured at 28 and 60 days were 27 MPa and 30 MPa, respectively. The longitudinal reinforcement and stirrups used in the column and transverse beam were made of deformed bars with a yield strength (f_y) of 440 MPa, tensile strength (f_u) of 700 MPa, and a modulus of elasticity of 200,000 MPa. The specimens were designed with specific dimensions, reinforcement configurations, and material properties, as outlined in the test matrix shown in Table 2. The formulae used are as follows:

$$V_{jh,u} = T - V_{col} \quad (2)$$

$$V_{n,ACI} = \sqrt{f_c'}A_j \quad (3)$$

$$L_{dh,ACI} = \frac{f_y d_b}{5.4\sqrt{f_c'}} \quad (4)$$

$$M_R = \frac{\Sigma M_c}{\Sigma M_b} \geq 1.2 \quad (5)$$

where $V_{jh,u}$, $V_{n,ACI}$, $L_{dh,ACI}$, and M_R represent the horizontal joint shear force, the nominal joint strength, the minimum anchorage length, and the ratio of the nominal moment capacity of the column to that of the beams, respectively. Meanwhile, T is the tensile force in the beam longitudinal reinforcement, V_{col} is the column shear force, f_c' is the concrete cylinder's compressive strength, d_b is the beam rebar diameter, ΣM_c is the sum of the nominal flexural strengths of the columns framing into the joint, and ΣM_b is the sum of the nominal flexural strengths of the beams framing into the joint.

The specimens were tested using a hydraulic actuator that applied a reverse cyclic lateral load at one end of the column. In this context, the loading sequence followed the quasi-static test procedure specified in ACI Code 374.1-05 [23], as shown in Figure 3. To simulate the effects of gravity loads on the joint, a 300 kN axial load (0.01Ag f_c') was applied at the column end using hydraulic jacks mounted on a rigid frame setup.

Details of the instrumentation setup, including the placement of linear variable differential transformer (LVDT) and strain gauges, are shown in Figures 4 and 5. These sensors were installed at designated locations to capture displacement and strain responses during testing.

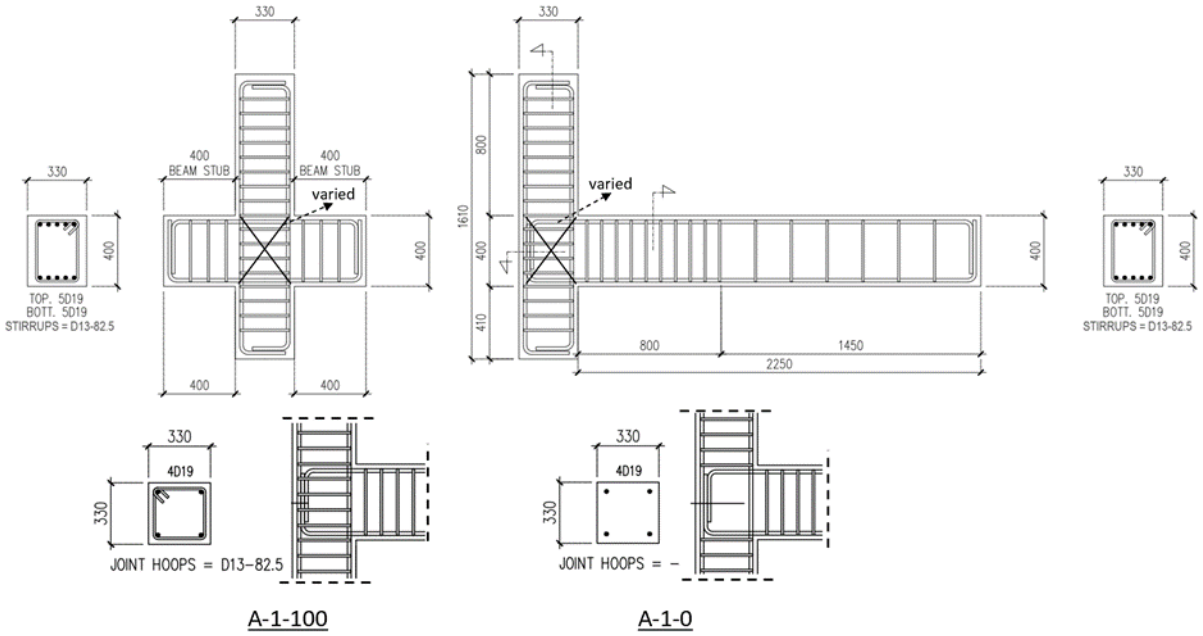

Fig. 2 Reinforcement details of specimens A-1-100 and A-1-0 (Note: all dimensions are in millimeters).

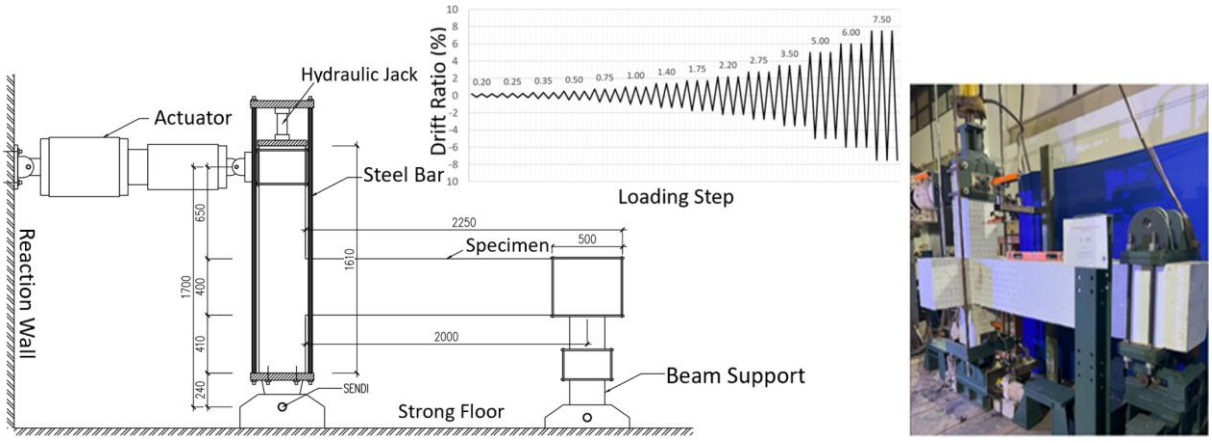

(a) (b)

Fig. 3 Experimental Setup (a) loading Arrangement and (b) test rig. (Note: all dimensions in millimeters).

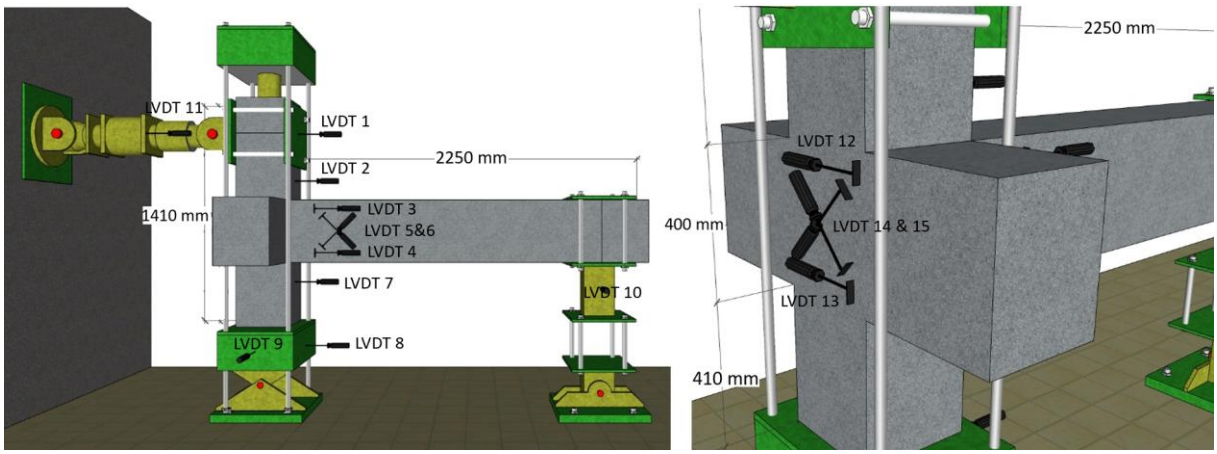

Fig. 4 Locations of LVDTs on the specimens.

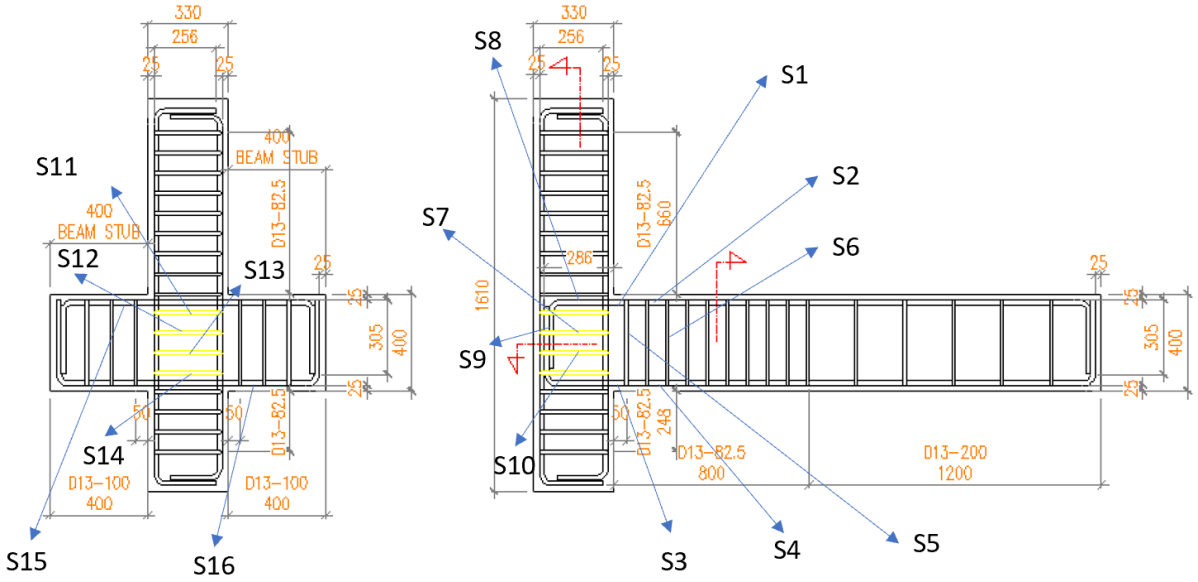

Fig. 5 Location of strain gauges on the specimens.

Table 2. Test matrix.

Specimen	f_c' (MPa)	f_y (MPa)	Column Dimension (mm)	Beam Dimension (mm)	$A_{sh\text{-}exp}/A_{sh\text{-}ACI}$	M_R	$V_{jh,u}/V_{n\text{-}ACI}$	$L_{dh}/L_{dh\text{-}ACI}$
A-1-0	27	440	330 × 330	400 × 330	0	1.58	1.07	1.01
A-1-100	27	440	330 × 330	400 × 330	1.73	1.58	1.07	1.01

5. RESULTS AND DISCUSSION

5.1 Experimental Observations and Hysteresis Response

Joint shear strength calculations indicated that the specimens had insufficient joint shear capacity and would typically end in joint failure (JF). However, the experimental results revealed a different outcome. Instead of experiencing pure JF, both specimens exhibited beam–joint failure (BJF), in which the beam's longitudinal reinforcement yielded before complete JF occurred. In this failure mode, observed in A-1-100 and A-1-0, significant damage developed on the rear side of the joint before the beam could form a full plastic hinge. Figures 6 and 7 show the relationships between the applied lateral load and drift ratio for all specimens, providing further insight into these observed failure patterns.

The hysteresis curve in Figure 6 indicates that cracks did not form in the joint of A-1-100 during the early stages of loading. However, when the drift ratio reached 1%, cracks appeared in the corner area and the rear side of the joint. These cracks rapidly widened from 0.25 mm to 5 mm at a 3.5% drift ratio This expansion occurred simultaneously with the development of the beam's flexural strength. Despite the joint's insufficient shear strength, the specimen sustained the yield strength of the beam reinforcement up to a 2% drift ratio. In this context, failure was characterized by volumetric expansion at the rear side of the joint and fracture of the concrete core. At a 5% drift ratio, the maximum lateral load caused significant damage, resulting in an outward displacement of 8.5 mm at the rear side of the joint, as shown in Figure 8(a).

Specimen A-1-0 displays a satisfactory hysteretic response even with the absence of horizontal joint reinforcement and insufficient shear strength, as shown in Figure 7. Beam yielding was observed at drift ratio of 1.4%, occurring earlier than joint damage. At this drift ratio, cracks with widths ranging from 0.5 to 1 mm appeared at the joint corners, indicating significant deformation. The key points on the hysteresis curve, such as initial cracking and yielding, followed a trend similar to A-1-100, but at lower drift ratio. As the drift ratio increased to 3.5%, extensive horizontal and vertical cracking developed in the joint core, with crack widths over 5 mm.

Compared to A-1-100, specimen A-1-0 developed a higher number of cracks with wider

openings. Aside from the higher cracks, the out-of-plane movement at the rear side of the joint exceeded 13.5 mm (0.53 in), causing failure in the form of volumetric expansion toward the rear side of the joint and fracture of the concrete core, as shown in Figure 8(b). A similar failure pattern was also reported in the studies by Kuang and Wong [12] and Pampanin *et al*. [19], where the absence of confinement at the rear side of the joint due to limited contribution from both concrete and transverse reinforcement led to significant out-of-plane deformation and degradation of joint integrity.

As previously shown in Figures 1, despite insufficient joint shear strength and variation in joint hoops, specimens A-1-100 and A-1-0 still exhibited high maximum drift ratios and ductility levels. The failure mechanism remained within the BJF mode, indicating that the beam was able to develop a plastic hinge. This pattern is comparable to the observations reported by Hwang *et al*. [5] and Ehsani and Wight [14], where deficiencies in joint hoops and joint shear strength did not prevent the specimens from showing a satisfactory hysteretic response. These comparisons demonstrate that strength hierarchy, reflected in the moment ratio, and adequate detailing are key factors influencing seismic performance.

Table 3 presents the joint strength ratios and cumulative energy dissipations of both specimens. The experimental shear strengths were compared with the predicted values based on the ACI 318-25 [1] design code, resulting in $V_u/V_{n\text{-}ACI}$ ratios of 0.97 for specimen A-1-0 and 1.01 for specimen A-1-100. These values indicate slight deviations, considering the initial assumptions used in the calculations. The cumulative energy dissipation of both specimens was relatively similar, with a difference of approximately 3.5%, which can be attributed to the failure mechanism governed by the yielding of the main beam reinforcement.

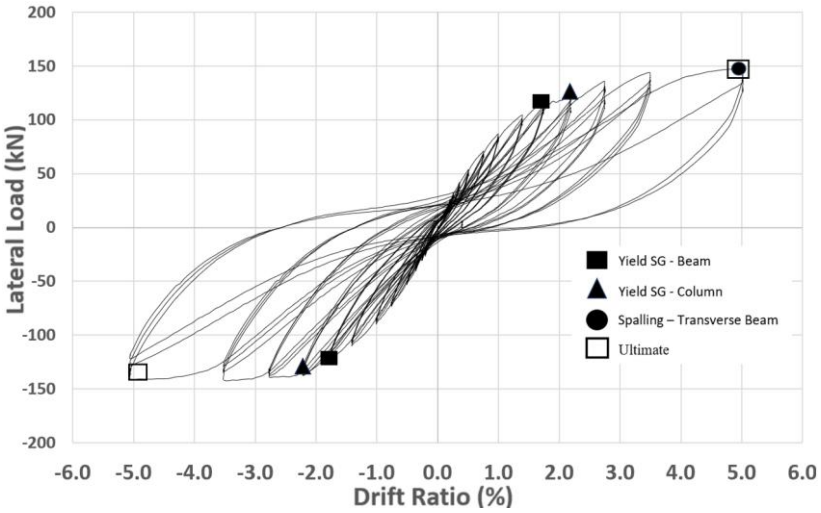

Fig. 6 Hysteretic response of specimen A-1-100

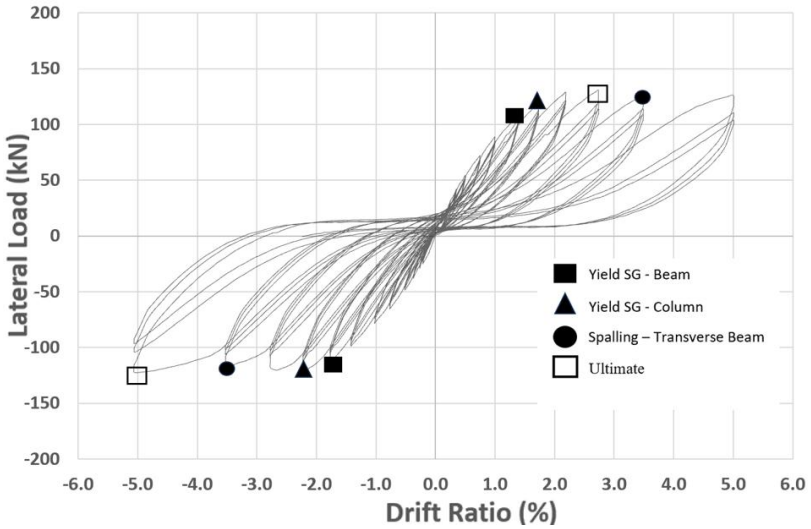

Fig. 7 Hysteretic response of specimen A-1-0.

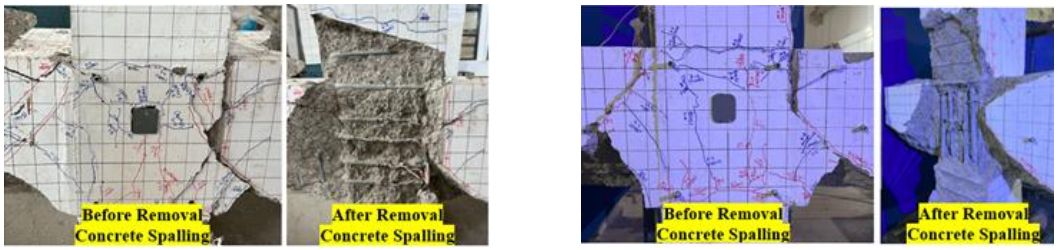

(a) (b)

Fig. 8 Damage patterns observed at 5% drift ratio and the final condition after testing: (a) specimen A-1-100 and (b) specimen A-1-0.

Table 3. Test results summary.

Specimen	P_y (kN)	Δ_y (%)	P_{max} (kN)	D_{max} (%)	μ (D_{max}/D_y)	Cumulative Energy Dissipation (kN.mm)	$V_{jh,u}/V_{n\text{-}ACI}$	Failure Mode
A-1-100	86.93	1.02	147.32	5.00	4.90	61,906.23	1.01	BJF
A-1-0	72.29	1.03	129.21	2.75	2.67	59,051.11	0.97	BJF

5.2 Role and Contribution of Side and Back Hoops Based on Measured Strain

The strain behavior of the side and back hoops was analyzed using embedded sensors to determine when and how these reinforcement elements engaged during different stages of structural response. As shown in Figure 9, the side and back hoops did not actively contribute to resisting the applied forces at the initial drift stages (<0.75%). Their effect became noticeable once the drift ratio exceeded 0.75%, as strain readings indicated activation of the side hoops. This early activation suggests that the side hoops primarily functioned to resist shear forces acting along the lateral sides of the joint.

As the drift ratio increased up to 2.75%, the side hoops played an increasingly significant role, as reflected in the rising strain values. During this phase, cracks began to develop at the rear and corners of the joint, as shown in Figure 10. The appearance of cracks suggested that the side hoops effectively resisted shear forces within the joint core until this stage. However, beyond the 2.75% drift ratio, the stress contribution from the back hoops began to increase and eventually exceeded that of the side hoops. This transition explains the shift in the joint's load-resisting mechanism, where confinement became a more dominant factor as deformations intensified.

At a 5% drift ratio, severe cracking occurred at the rear joint corners (Figure 11). The back hoops became critical in limiting dilation and distortion, with strain readings exceeding 0.002, indicating they had yielded and confirming their essential role in maintaining joint integrity under large deformations.

Unlike the back hoops, the contribution of the side hoops decreased with increasing drift ratio, likely due to bond degradation caused by cracking at the joint corners. Strain data showed that the side hoops reached a maximum strain of 0.0015, below the yield strain, indicating limited effectiveness in resisting shear. As damage progressed, the back hoops played a more dominant role by maintaining confinement and preserving joint integrity at higher drift ratios.

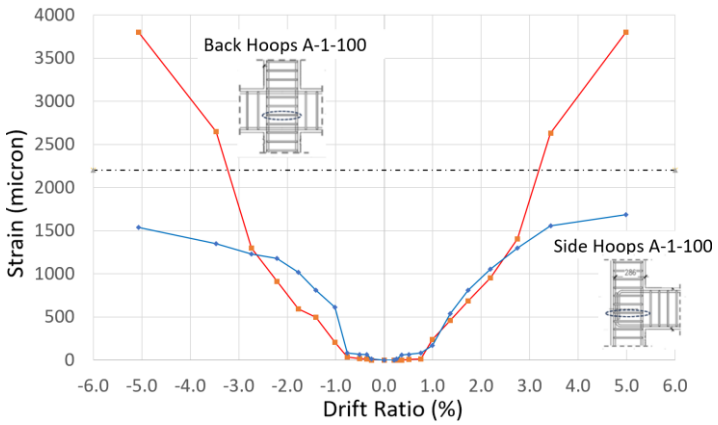

Fig. 9 Measured strain in side and back joint hoops of specimen A-1-100.

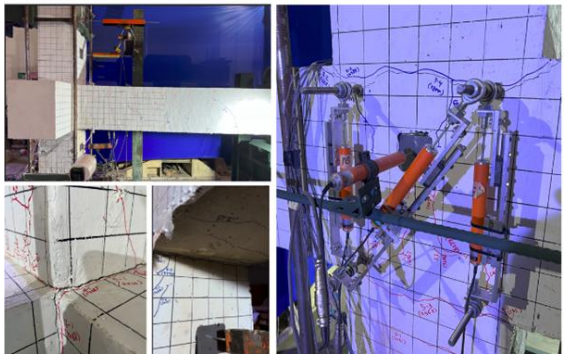

Fig. 10 Crack pattern at 2.75% drift ratio for specimen A-1-100.

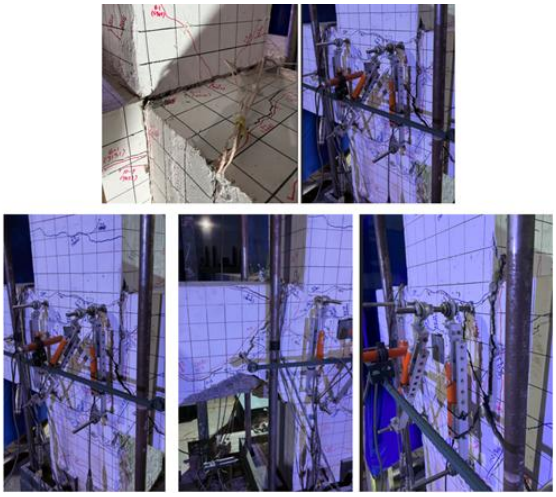

Fig. 11 Crack pattern at 5% drift ratio for specimen A-1-100.

5.3. Contribution of Truss and Strut Mechanisms in Joint Behavior

Building on the previous discussion, the side hoops played a crucial role in resisting both shear and dilation, while the back hoops primarily contributed to controlling dilation. To further understand the load transfer behavior within the joint, the joint strength mechanisms in the experimental specimens were examined. According to Park and Paulay [17], as well as the New Zealand approach, joint strength is governed by two mechanisms: truss and strut. Specifically, the truss mechanism relies on reinforcement to transfer shear forces, while the strut mechanism involves diagonal compression in the concrete core that facilitates force transfer. The interaction between these mechanisms determines the overall joint performance under seismic loading.

To quantify the contribution of each mechanism at different drift ratios or loading cycles for specimens A-1-100 and A-1-0, calculations were performed using specific equations. The truss mechanism (V_{truss}) was determined as the sum of $V_{side\text{-}hoops}$ and $V_{back\text{-}hoops}$, with these values obtained by converting strain gauge measurements into forces acting on each hoop reinforcement:

$$V_{truss} = V_{side-hoops} - V_{back-hoops} \quad (6)$$

The contribution of the strut mechanism (V_{strut}) was determined by subtracting the reinforcement force contribution from the total shear demand (V_{joint}):

$$V_{joint} = V_{truss} + V_{strut} \text{ and} \quad (7)$$

$$V_{strut} = V_{joint} - V_{truss} \quad (8)$$

A summary of the results is presented in Table 4.

Figure 12 shows the truss mechanism in specimen A-1-100 can be divided into two regions based on the drift ratio. In the first region, where the drift ratio remained below 2%, the contribution of the truss mechanism progressively increased. During this phase, the joint remained relatively intact, exhibiting minimal cracking and deformation. The bond between the reinforcement and concrete was still effective, allowing the truss mechanism to efficiently transfer shear forces.

In the second region, when the drift ratio exceeded 2%, the contribution of the truss mechanism gradually declined. This reduction was primarily attributed to the progressive degradation of bonding between the reinforcement and the surrounding concrete, which weakened the mechanism's capacity to transfer shear forces. As the bond continued to degrade, the truss mechanism became less effective. Consequently, the load-resisting behavior shifted, with the strut mechanism playing a more dominant role in maintaining joint stability.

Figure 13 presents the proportions of the strut and truss mechanisms at various drift ratios. During the initial stage, the truss mechanism contributed approximately one-third of the total joint resistance. This trend remained consistent up to the DBE-level drift ratio limit of 2%, where the truss mechanism reached its peak contribution of approximately 30%, while the strut mechanism accounted for the remaining 70%. These findings indicate that, up to this drift limit, the truss mechanism significantly contributed to joint strength.

At higher drift ratios, particularly at the MCE_R limit of 3%, the contribution of the truss mechanism decreased to 17%, while that of the strut mechanism increased to 83%. This shift signified that the concrete strut mechanism governed the joint's resistance, as the effectiveness of the truss mechanism was diminished due to the progressive bond degradation within the specimen. This observation with the ACI 318-25 approach, which excludes the truss mechanism from joint strength calculations, acknowledging its limited under inelastic demands.

Table 4. Truss and strut contributions at various drift ratios for Specimen A-1-100 and A-1-0.

Drift Ratio (%)	Specimen A-1-100					Specimen A-1-0
	$V_{side\text{-}hoops}$ (kN)	$V_{back\text{-}hoops}$ (kN)	V_{truss} (kN)	V_{joint} (kN)	V_{strut} (kN)	V_{strut} (kN)
0	0	0	0	0.00	0.00	0.00
0.5	13.80	0.00	13.80	229.25	215.45	231.46
1	129.91	21.65	108.25	369.45	261.20	378.51
1.5	193.37	52.43	140.94	476.00	335.06	467.50
1.75	215.66	62.94	152.72	495.25	342.53	482.55
2.2	250.47	96.90	153.57	534.82	381.25	515.95
2.75	260.66	137.97	122.69	573.03	450.34	557.60
3.5	286.56	238.27	48.29	609.32	561.03	535.50
5	326.04	291.86	34.17	626.11	591.94	531.25

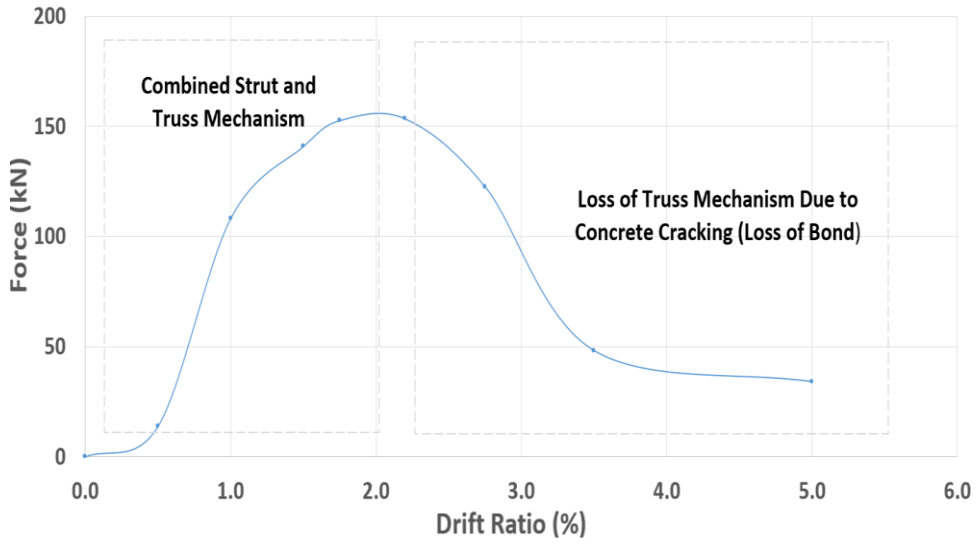

Fig. 12 Development of a truss mechanism in specimen A-1-100.

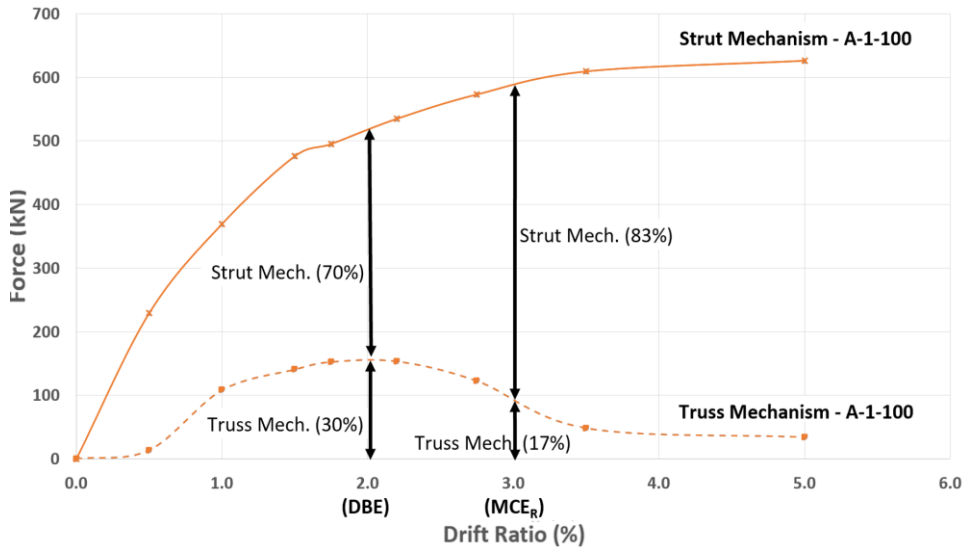

Fig. 13 Contribution of strut and truss mechanisms in specimen A-1-100.

6. CONCLUSIONS

This study evaluated the performance of beam–column joints (BCJ) through experimental testing and database analysis. Among the 59 database specimens, most sustained drift ratios exceeding 2% under design-basis earthquake demands and demonstrated deformability up to 3.5% under maximum considered earthquake conditions. Experimental results showed that, even without joint hoops, specimen A-1-0 exhibited ductile behavior, suggesting that strict compliance with hoop requirements in ACI 318-25 may be conservative for certain exterior BCJs.

The contribution of joint hoops varied with drift ratio. At lower drift ratios, side hoops were effective in resisting shear and controlling dilation. However, their effectiveness diminished with crack propagation. Conversely, back hoops became increasingly important at higher drift ratios by providing confinement and ensuring structural integrity.

For specimen A-1-100, a shift in the joint resistance mechanism was observed. At drift ratios below 2%, the truss mechanism contributed up to 30% of the total joint strength, while the strut mechanism carried the remaining 70%. As the drift ratio increased beyond 2%, the truss mechanism degraded because of bond loss, reducing its contribution to 17% at a 3.5% drift ratio. The strut mechanism then became dominant, aligning with ACI 318-25 provisions, which exclude the truss mechanism in joint strength prediction.

These findings highlight the potential to optimize the number of joint hoops without compromising seismic performance, provided that other requirements such as the moment ratio and anchorage length are met. The results offer experimental support for performance-based design approaches and deepen the understanding of internal force mechanisms in BCJs. However, the relatively small number and limited variation of tested specimens remain key limitations, potentially affecting the generalizability of the findings to a broader range of joint configurations.

Future studies are encouraged to include numerical simulations to validate the observed trends and extend the parameter space beyond what is feasible in laboratory settings. Additionally, investigations of retrofit strategies for substandard joints could further support the development of practical and cost-effective strengthening approaches.

7. ACKNOWLEDGMENTS

The authors are grateful to Institut Teknologi Bandung (ITB) for their financial support. This study was made possible through funding provided under the Research Centers of Excellence (RU3P) program and the Research, Community Service, and Innovation (PPMI) ITB program. The support from these programs significantly contributed to both the experimental and analytical aspects of this work.

8. REFERENCES

[1] ACI Committee 318, Building Code for Structural Concrete – Code Requirements and Commentary, American Concrete Institute, Farmington Hills, Mich, 2025.

[2] ACI Committee 352R-02, Recommendations for Design of Beam-Column Connection in Monolithic Reinforced Concrete Structures, American Concrete Institute, Farmington Hills, Mich, 2002.

[3] Meinheit D. F., and Jirsa J. O., Shear Strength of Reinforced Concrete Beam-Column Joints, Department of Civil Engineering, Structures Research Laboratory, University of Texas at Austin, Report No. 77–1, 1977.

[4] Hirosawa M., Strength and Ductility of Reinforced Concrete Members in Japanese, Report of the Building Research Institute, Issue 76, 1977, pp. 1967–1974.

[5] Hwang S. J., Lee H. J., Liao T. F., Wang K. C., and Tsai, H. H., Role of Hoops on Shear Strength of Reinforced Concrete Beam-Column Joints, ACI Structural Journal, Vol. 102, Issue 3, 2005, pp. 445–453.

[6] Al-Osta M. A., Khan U., Baluch M. H., and Rahman M. K., Effects of Variation of Axial Load on Seismic Performance of Shear Deficient RC Exterior BCJs, International Journal of Concrete Structures and Materials, Vol. 12, Issue 46, 2018.

[7] Castro J. J., and Imai H., Structural Performance of Exterior Beam-Column Joint with Mechanical Anchorage at Main Bars, 13th World Conference on Earthquake Engineering, Vancouver, B.C., Canada, Issue August 1–6, 2004.

[8] Alaee P., and Li B., High Strength Concrete Exterior Beam-Column Joints with High Yield Strength Steel Reinforcements, Engineering Structures, Vol. 145, 2017, pp. 305–321.

[9] Hwang H. J., and Park H. G., Performance-Based Shear Design of Exterior Beam-Column Joints with Standard Hooked Bars, ACI Structural Journal, Vol. 117, Issue 2, March 2020, pp. 67–80.

[10] Huang R. Y. C., Kuang J. S., and Mogili S., Effect of Joint Hoops on Seismic Behavior of Wide Beam-Column Joints, ACI Structural Journal, Vol. 116, Issue 6, November 2019, pp. 131–142.

[11] Hakuto S., Park R., and Tanaka H., Seismic Load Tests on Interior and Exterior Beam-

Column Joints with Substandard Reinforcing Details, ACI Structural Journal, Vol. 97, Issue 1, 2000, pp. 47–59.

[12] Kuang, J. S., and Wong, H. F., Effectiveness of Horizontal Stirrups in Joint Core for Exterior Beam-Column Joints with Nonseismic Design, Procedia Engineering, Vol. 14, 2011, pp. 1877–7058.

[13] Lee H. J., and Chang C. J., High-Strength Reinforcement in Exterior Beam-Column Joints under Cyclic Loading, ACI Structural Journal, Vol. 114, Issue 5, 2017, pp. 1325–1338.

[14] Ehsani M. R., and Wight J. K., Exterior Reinforced Concrete Beam-to-Column Connections Subjected to Earthquake-Type Loading, ACI Journal, Vol. 82, Issue 4, 1985, pp. 492–498.

[15] Canbolat B. B., and Wight J. K., Experimental Investigation on Seismic Behavior of Eccentric Reinforced Concrete Beam-Column Slab Connection, ACI Structural Journal, Vol. 105, Issue 2, 2008, pp. 154–162.

[16] Lee H. J., and Yu S. Y., Cyclic Response of Exterior Beam-Column Joints with Different Anchorage Methods, ACI Structural Journal, Vol. 106, Issue 3, 2009, pp. 329–339.

[17] Park R., and Paulay T., Reinforced Concrete Structures, John Wiley & Sons, New York, 1975.

[18] Alshayed S. H., Al-Salloum Y. A., Almusallam T. H., and Siddiqui N. A., Seismic Response of FRP-Upgraded Exterior RC Beam-Column Joints, Journal of Composites for Construction, ASCE, Vol. 14, 2010, pp. 195–208.

[19] Pampanin S., Calvi G. M., and Moratti M., Seismic Behaviour of R.C. Beam-Column Joints Designed for Gravity Loads, 12th European Conference on Earthquake Engineering, Elsevier Science Ltd., Paper Reference 726, 2002.

[20] Bindhu K. R., and Sukumar P. M., Performance of Exterior Beam-Column Joints Under Seismic Type Loading, ISET Journal of Earthquake Technology, Vol. 46, Issue 2, 2009, pp. 47–64.

[21] Paulay T., and Scarpas A., The Behaviour of Exterior Beam-Column Joints, Bulletin of the New Zealand National Society for Earthquake Engineering, Vol. 14, No. 3, September 1981, pp. 131–144

[22] Wibowo A., and Cahyani R. A. T., Structural Behavior of Non-Ductile Reinforced Concrete Columns, International Journal of GEOMATE, Vol. 19, Issue 73, 2020, pp. 201–207.

[23] ACI Committee 374, Acceptance Criteria for Moment Frames Based on Structural Testing and Commentary (Reapproved 2019) (ACI 374.1-05(19), American Concrete Institute, Farmington Hills, MI, 2019.